Computers and Geotechnics 190 (2026) 107681

Contents lists available at ScienceDirect

Computers and Geotechnics

journal homepage: www.elsevier.com/locate/compgeo

A thermodynamic-based macroelement framework for soil-foundation systems with coupled hydro-mechanical behaviour

Davide Noè Gorini [a,*], Giuseppe Lombardi [b], Luigi Callisto [b]

[a] University of Trento, Italy
[b] Sapienza University of Rome, Italy

ARTICLE INFO

Keywords:
Multiaxial soil-structure interaction
Excess pore water pressure
Hyper-elasticity
Hyper-plasticity
Cyclic degradation

ABSTRACT

The plasticity-based macroelement approach for simulating soil-structure interaction in the analysis of structures is rapidly extending by virtue of its efficient balance between accuracy and computational demand. This approach has been mostly developed neglecting the effect of any excess pore water pressures produced by load cycles which can be, however, somewhat unrealistic in the case of saturated soils under dynamic loading. To overcome this long-standing limitation, the present paper develops a formulation comprising the effects of the hydro-mechanical coupling of the soil behaviour on the multiaxial foundation response. This is handled through a consistent thermodynamic framework, in which the time evolution of the stiffness and resistance of the macroelement is controlled by an internal variable accounting for drainage conditions. A complementary damage variable simulates the temporary degradation of the macroscopic mechanical features induced by the pore water pressure build-up. The macroelement is tested under different conditions, highlighting the importance of the coupled hydro-mechanical soil behaviour on the foundation performance.

1. Introduction

Soil-structure interaction is receiving an increasing attention for its strong impact on design of civil engineering structures against static and dynamic load patterns. The response of the soil region interacting with the structure (called *participating soil* from here on) can indeed alter the structural performance because of peculiar nonlinear and frequency-dependent features. This can even cause detrimental effects in several circumstances, due to i) the prominent inertial effects developing in the participating soil under dynamic loading (e. g., Elgamal et al., 2008; Kotsoglou and Pantazopoulou, 2007; Kotsoglou and Pantazopoulou, 2009; Waldin et al., 2012; Rahmani et al., 2014; Taskari and Sextos, 2015; Gorini and Callisto, 2020; Gorini et al., 2022; Gorini and Callisto, 2023; Gorini et al., 2023; Gallese et al., 2023; Franchin et al., 2023) or ii) the alteration of the foundation response induced by the hydro-mechanical coupling of the soil behaviour.

In the presence of saturated foundation soils, cyclic perturbations can produce excess pore water pressures in the foundation soils. This may induce critical effects in the geotechnical system, such as a reduction in the ultimate capacity and the deterioration of the resistance and stiffness with the number of cycles (Cascone and Bouckovalas, 1998; Karamitros et al., 2013a; Karamitros et al., 2013b; Casablanca et al., 2023; Lombardi et al., 2024). These effects are accompanied by the accumulation of irreversible displacements and by a permanent increase of internal forces in the structural members (Liu & Dobry 1997; Dashti et al., 2010, Bazaios et al., 2023).

Despite numerous efforts devoted in the past to the understanding of the above effects, the insertion of the effect of drainage conditions into a soil-structure interaction analysis still entails coupled numerical representations of the entire soil-structure layout. In turn, this implies a refined description of the soil behaviour, which can be warranted only for specific cases of major importance. To overcome this limitation, this paper explores the possibility of extending the macroelement approach (Roscoe, 1956; Nova and Montrasio, 1991) to include at the macroscopic scale the effect of the development of excess pore water pressures in the foundation soil under cyclic loading conditions. To the authors' knowledge, in the past the only attempts to follow this path were those published by Flessati et al. (2021), as a one-dimensional macroelement for shallow footings resting on fine-grained soils and loaded monotonically, and by Peccin da Silva et al. (2023) with specific reference to the cyclic response of plate anchors.

The present work proposes a practice-oriented model to account for

* Corresponding author.
E-mail address: davidenoe.gorini@unitn.it (D.N. Gorini).

https://doi.org/10.1016/j.compgeo.2025.107681
Received 13 May 2025; Received in revised form 26 September 2025; Accepted 1 October 2025
Available online 16 October 2025
0266-352X/© 2025 The Authors. Published by Elsevier Ltd. This is an open access article under the CC BY-NC-ND license (http://creativecommons.org/licenses/by-nc-nd/4.0/).

the coupled hydro-mechanical (UP) response of a class of geotechnical systems in the numerical analysis of buildings and bridges at a residual computational effort. This is accomplished by including the UP response into the thermodynamic-based macroelement framework for soil-foundation systems recently developed by Gorini (2025). The latter consists of a unified macroelement, named TIM-G, formulated in compliance with the Principles of Thermodynamics to simulate the nonlinear and frequency-dependant response of geotechnical systems under general load patterns (three forces and three moments exchanged with the superstructure). The power and elegance of a thermodynamic framework, also referred to as hyperplasticity (Collins and Houlsby, 1997; Houlsby and Puzrin, 2000a; Houlsby and Puzrin, 2000b; Houlsby and Puzrin, 2006), are evidenced by its increasing use in interpreting and solving geomechanical problems at both the meso- and macro-scales (Le Pape and Sieffert, 2001; Einav and Cassidy, 2005; Nguyen-Sy, 2005; Houlsby et al., 2017).

The paper is structured as follows: an overview to the UP approach is introduced in Section 2, Section 3 describes the formulation and calibration of the macroelement, whereas its potentialities are tested in Section 4. Conclusive remarks are provided in Section 5.

2. From the TIM-G to the TIMg-UP framework

In this paper, the 6D Thermodynamic Inertial Macroelement proposed by Gorini (2025), named TIM-G, is substantially renewed with an extended formulation, termed TIMg-UP, accounting for the hydro-mechanical behaviour of saturated soils. An overview to the formal structure, the applicability of the TIMg-UP and the steps forward compared to the TIM-G formulation is reported in Table 1.

The TIMg-UP aims at simulating the response of shallow, piled, monopile and caisson foundations, on horizontal or sloping ground; semi-integral and integral seat- or cantilever-type bridge abutments, resting on shallow or deep foundations. It lumps the response of the foundation and of the participating soil into a single constitutive relationship between the generalised forces, Q_i, exchanged at the foundation-superstructure contact and the corresponding displacements and rotations, q_i, considering directions i as in Fig. 1 (i = 1, 2 refers to horizontal translations, i = 3 is the vertical translation, i = R1, R2, R3 are the rotations around axes 1, 2 and 3, respectively). The incremental relationship reads:

$$\dot{Q}_i = H_{ij} \bullet \dot{q}_j \tag{1}$$

in which H_{ij} is the second-order tangent stiffness matrix. The rate of deformation in the i^{th} degree of freedom is given as:

$$\dot{q}_i = \dot{q}_i^{(0)} + \sum_{n=1}^{N} \dot{q}_i^{(n)} + \dot{q}_i^{(R)} \tag{2}$$

where $q_i^{(k)}$ represents, when $k = 0$, the elastic deformation in the i-direction and, for $k = 1,2,\ldots,N$, the k^{th} plastic deformation associated with the attainment of the k^{th} yield surface; $q_i^{(R)}$ is an additional plastic deformation simulating ratcheting of the geotechnical system (see, for instance, Houlsby et al., 2017). The TIMg-UP incorporates distinct hydro-mechanical effects at the scale of the geotechnical system, as observed in recent works (Lombardi et al., 2024; Lombardi, 2025), namely: i) the dependence of the stiffness and resistance on drainage conditions, ii) a degradation of the response induced by the load cycles, as a phenomenological effect of the pore water pressure build-up occurring at the *meso*-scale.

The use of the TIMg-UP in a time-domain analysis of a structure follows the procedure schematised in Fig. 1, taking seismic loading as a reference: the ground motion is propagated through the foundation soils by means of a free-field site response analysis taking into consideration the presence of the pore water pressure build-up; the resulting motion at an effective depth from the foundation (Gorini et al., 2023; Gorini and Callisto, 2023; Gorini, 2025) represents the seismic input for the TIMg-UP inserted at base of the structural model.

3. Analytical framework

The TIMg-UP is a multi-surface plasticity (Prevost, 1978) model featuring a mixed kinematic and isotropic hardening, simulating the hysteretic response under cyclic loading and the dependence of the available resistance on drainage conditions. The macroelement is composed of N yield surfaces defined in the generalised force space. The plastic response activates in correspondence of the surface of first yield ($n = 1$), while the admissible force combinations are bounded by the surface of ultimate loads (n=N). For force states internal to the first surface the behaviour is nonlinear hyper-elastic.

The incremental form in Eqs. (1) and (2) is developed within a thermodynamic-based framework with internal variables, completely derived by two potentials, i.e., the free energy and dissipation functions, which guarantee the consistency of deformation processes with the Principles of Thermodynamics. The potentials include distinct features of the monotonic and cyclic response of geotechnical systems, that are: material nonlinearity, multiaxiality, the strong dependence on the load direction, the macroscopic effects of the coupled hydro-mechanical soil behaviour.

3.1. Energy function

The energy function can be expressed as the Helmholtz free energy, ψ, or equivalently through the Gibbs free energy, g. These are state quantities correlated by the Legendre transform, such that $\psi + g = Q_i \bullet q_i$. In the TIMg-UP, the energy function of the TIM-G encloses additional internal variables relating to the hydro-mechanical coupling of the soil behaviour. The extended free energy assumes the following form:

$$\psi = \psi_D \bullet U + \psi_U \bullet (1 - U) \tag{3}$$

Table 1
Comparison between the TIM-G and the TIMg-UP (novel aspects in bold).

Formulation	TIM-G	TIMg-UP
Applicability	Shallow foundationsPiled foundations (with soil-raft contact)Caisson foundations (horiz. or sloping ground) Monopile foundations Seat- or cantilever-type abutments with shallow or deep foundations	Shallow foundationsPiled foundations (with soil-raft contact)Caisson foundations (horiz. or sloping ground) Monopile foundations Seat- or cantilever-type abutments with shallow or deep foundations
Load combinations	Full pattern, Q_1-Q_2-Q_3-Q_{R1}-Q_{R2}-Q_{R3}	Full pattern, Q_1-Q_2-Q_3-Q_{R1}-Q_{R2}-Q_{R3}
Energy function	Unified	Unified
Dissipation function	Unified	Unified
Small-strain response	Linear elastic	**Nonlinear hyper-elastic**
Hardening	Kinematic	**Kinematic and isotropic**
Hydro-mech. coupling	Neglected	**Considered, through a thermodynamic-based extension of the potential functions**

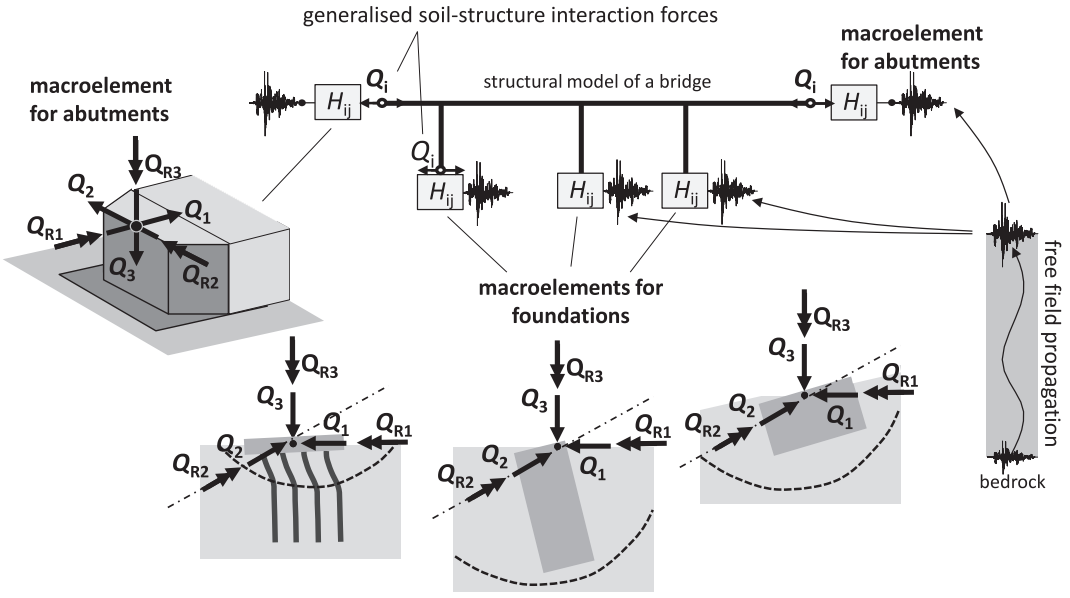


Fig. 1. Application of the TIMg-UP in the seismic analysis of a bridge and applicability to different geotechnical systems.

which is composed of the drained and undrained (subscripts D and U, respectively) contributions to the system response. The internal variable U is a scalar function simulating reversible macroscopic effects of the evolving drainage conditions in the foundation soil. It varies from 0 to 1, corresponding to fully undrained and fully drained response, respectively. The U-related free energy ψ_U is in turn composed of two distinct contributions, such that:

$$\psi_U = \psi_U^{(0)} \bullet (1 - C) + \psi_U^{(C)} \bullet C \tag{4}$$

where C is a damage-like internal variable that simulates the cycle-by-cycle degradation in the stiffness and resistance of the geotechnical system. More specifically, C controls the transition between a non-degraded undrained response (named U0, corresponding to $C = 0$) and a residual undrained condition of the geotechnical system (UC, $C = 1$).

The conditions U0 and UC have a straightforward connection with the *meso*-scale behaviour. The former represents a reversible condition (no degradation) caused by the variations of the mean total stress in the foundation soil, in turn induced by the pore water pressure build-up. Cyclic degradation can be instead ascribed to the volumetric-deviatoric coupling of the soil behaviour (see, for instance, Lombardi et al., 2024), producing for $U < 1$ a dissipative alteration of the response, which vanishes when U tends back to unity. Degradation under undrained loading is therefore regarded as an additional energy contribution to the system response, controlled by C, whose effect is weighted by the level of hydro-mechanical coupling, U.

Accordingly, the Helmholtz free energy reads:

$$\psi = \psi_D \bullet U + \left[\psi_U^{(0)} \bullet (1 - C) + \psi_U^{(C)} \bullet C\right] \bullet (1 - U) \tag{5}$$

in which functions ψ_k have the following analytical structure:

$$\psi_D = \left[\frac{1}{2} \bullet H_{D,ij}^{(0)} \bullet \left(q_j - \sum_{n=1}^{N} q_j^{(n)} - q_j^{(R)}\right) \bullet \left(q_i - \sum_{n=1}^{N} q_i^{(n)} - q_i^{(R)}\right)\right]^m + \frac{1}{2} \bullet \sum_{n=1}^{N} H_{D,ij}^{(n)} \bullet q_j^{(n)} \bullet q_i^{(n)} \tag{6}$$

$$\psi_U^{(p=0,C)} = \left[\frac{1}{2} \bullet H_{U,ij}^{(0,p)} \bullet \left(q_j - \sum_{n=1}^{N} q_j^{(n)} - q_j^{(R)}\right) \bullet \left(q_i - \sum_{n=1}^{N} q_i^{(n)} - q_i^{(R)}\right)\right]^m + \frac{1}{2} \bullet \sum_{n=1}^{N} H_{U,ij}^{(n,p)} \bullet q_j^{(n)} \bullet q_i^{(n)} \tag{7}$$

where $H_{k,ij}^{(0)}$ is the elastic stiffness matrix relating to condition $k = D$, U (drained and undrained, respectively) and $H_{ij}^{(n)}$ is the stiffness matrix associated with the n^{th} yield surface. The first addendum represents the energetic contribution of the nonlinear hyper-elastic response within the first yield surface ($m = 1$ corresponds to the linear elastic case). In accordance with the macroscopic features of soil-foundation systems highlighted in Lombardi et al. (2024) and Lombardi (2025), nonlinear elasticity of the TIMg-UP is conceived to provide more realistic assessment i) of the hysteretic force–deformation loops under small cyclic perturbations and ii) of the variability of the system stiffness on the level of mobilised strength.

From Eqs. (5)-(7) one can obtain the Gibbs free energy using the Legendre transformation, such that:

$$g = Q_i^{(l)} \bullet q_i^{(l)} - \psi = \left(-\frac{1}{2} \bullet K_{eq,ij}^{(0)} \bullet Q_j^{(0)} \bullet Q_i^{(0)}\right)^{\frac{m}{2m-1}} - \sum_{n=1}^{N} Q_i^{(n)} \bullet q_i^{(n)} + \frac{1}{2} \bullet \sum_{n=1}^{N} H_{eq,ij}^{(n)} \bullet q_j^{(n)} \bullet q_i^{(n)} - Q_i^{(R)} \bullet q_j^{(R)} \tag{8}$$

where $K_{eq,ij}^{(l)}$ represents the resulting compliance matrix, including the contributions of the drained and undrained response, in the elastic regime ($l = 0$) and associated with the plastic flows ($l = n$). This matrix will be fully derived in Section 3.2, and can be written in the subsequent compact form:

$$K_{eq,ij}^{(l)} = H_{eq,ij}^{(l)-1} = \left[H_{U,ij}^{(l,0)} + C \bullet \left(H_{U,ij}^{(l,C)} - H_{U,ij}^{(l,0)}\right) + U \bullet \left(H_{D,ij}^{(l)} - H_{U,ij}^{(l,0)}\right) + U \bullet C \bullet \left(H_{U,ij}^{(l,0)} - H_{U,ij}^{(l,C)}\right)\right]^{-1} \tag{9}$$

Therefore, the internal variables are the plastic deformations, $q_i^{(n>0)}$ and $q_i^{(R)}$, U and C, which are linked to the force–deformation response of

the TIMg-UP through the thermodynamic-based formalism developed in the next sections.

3.2. Thermomechanical consistency

The first and second Laws of Thermodynamics are written below:

$$\dot{W} = \dot{\psi} + \dot{d} \tag{10}$$

$$\dot{d} \geq 0 \tag{11}$$

where $\dot{W}$ is the increment of the mechanical work of the TIMg-UP, $\dot{\psi}$ and $\dot{d}$ are the rates of the Helmholtz free energy and dissipation, respectively. The latter is assumed as a homogeneous function of degree one in the rates of the internal variables causing irreversible effects, such that:

$$\dot{d} = \sum_{n=1}^{N} \frac{\partial d}{\partial \dot{q}_i^{(n)}} \bullet \dot{q}_i^{(n)} + \frac{\partial d}{\partial \dot{q}_i^{(R)}} \bullet \dot{q}_i^{(R)} + \frac{\partial d}{\partial \dot{C}} \bullet \dot{C} \tag{12}$$

Introducing Eq. (5) and Eq. (12) into Eq. (10) and expressing the rate of the mechanical work as $\dot{W} = Q_i \bullet \dot{q}_i$, the first Law reads:

$$\left(Q_i - \frac{\partial \psi}{\partial q_i^{(0)}}\right) \bullet \dot{q}_i^{(0)} + \sum_{n=1}^{N} \left(Q_i - \frac{\partial \psi}{\partial q_i^{(n)}} - \frac{\partial d}{\partial \dot{q}_i^{(n)}}\right) \bullet \dot{q}_i^{(n)} - \left(\frac{\partial \psi}{\partial C} + \frac{\partial d}{\partial \dot{C}}\right) \bullet \dot{C} + \left(\frac{\partial \psi}{\partial q_i^{(R)}} - \frac{\partial d}{\partial \dot{q}_i^{(R)}}\right) \bullet \dot{q}_i^{(R)} = 0 \tag{13}$$

The dissipative forces arise from variables whose rates contribute to dissipation. For this reason, the Clausius-Duhem equation above is evaluated with respect to the rates $\dot{q}_i^{(0)}$, $\dot{q}_i^{(n>0)}$, $\dot{q}_i^{(R)}$ and $\dot{C}$.

The drainage variable U describes instead the state of the soil-foundation system (e.g., effective stiffness and resistance) accounting for the macroscopic drainage level in the foundation soil. It reproduces the reversible effects of the pore water pressure build-up, which lead to temporary variations in the macroscopic mechanical properties of the geotechnical system with respect to the fully drained condition. These variations vanish as soon as the excess pore water pressures dissipate.

The thermodynamic consistency must hold for each $\dot{q}_i^{(0)}$, $\dot{q}_i^{(n>0)}$, $\dot{q}_i^{(R)}$ and $\dot{C}$, so the following constitutive constraints can be identified through Eq. (13):

$$Q_i = \frac{\partial \psi}{\partial q_i^{(0)}} = \frac{\partial \psi}{\partial q_i^{(n)}} + \frac{\partial d}{\partial \dot{q}_i^{(n)}} = c_i^{(n)} + \chi_i^{(n)} \tag{14}$$

$$\chi^{(C)} = \frac{\partial d}{\partial \dot{C}} = -\frac{\partial \psi}{\partial C} \tag{15}$$

$$\chi_i^{(R)} = -\frac{\partial d}{\partial \dot{q}_i^{(R)}} = -\frac{\partial \psi}{\partial q_i^{(R)}} \tag{16}$$

where $\chi^{(C)}$ is named dissipative hydro-mechanical force (conjugated term of $\dot{C}$), $\chi_i^{(R)}$ is the dissipative ratcheting force and $\chi_i^{(n)} = \partial d / \partial \dot{q}_i^{(n)}$ is the n^{th} dissipative plastic force, that are the conjugated terms of the internal variables contributing to dissipation. So, $\chi_i^{(n)}$ represents the true force Q_i minus the translation of the centre with respect to the initial configuration of the n^{th} yield surface, $c_i^{(n)}$, called *back force* (Eq. (14)).

As a relevant case, when the behaviour is linear elastic within the first yield surface ($m = 1$ in Eqs. (6)-(7)), the true force vector assumes the following form:

$$\begin{aligned} Q_i &= \frac{\partial \psi_D}{\partial q_i^{(0)}} \bullet U + \left[\frac{\partial \psi_U^{(0)}}{\partial q_i^{(0)}} \bullet (1 - C) + \frac{\partial \psi_U^{(C)}}{\partial q_i^{(0)}} \bullet C\right] \bullet (1 - U) \\ &= H_{U,ij}^{(0,0)} \bullet \left(q_j - \sum_{n=1}^{N} q_j^{(n)} - q_j^{(R)}\right) + U \bullet \left(H_{D,ij}^{(0)} - H_{U,ij}^{(0,0)}\right) \\ &\quad \bullet \left(q_j - \sum_{n=1}^{N} q_j^{(n)} - q_j^{(R)}\right) + C \bullet \left(H_{U,ij}^{(0,C)} - H_{U,ij}^{(0,0)}\right) \\ &\quad \bullet \left(q_j - \sum_{n=1}^{N} q_j^{(n)} - q_j^{(R)}\right) + U \bullet C \bullet \left(H_{U,ij}^{(0,0)} - H_{U,ij}^{(0,C)}\right) \\ &\quad \bullet \left(q_j - \sum_{n=1}^{N} q_j^{(n)} - q_j^{(R)}\right) \\ &= Q_{D,i} + Q_{U,i} + Q_{C,i} + Q_{UC,i} \end{aligned} \tag{17}$$

It is composed of a term relating to the drained response, $Q_{D,i}$, a term producing reversible effects controlled by the level of drainage in the foundation soil, $Q_{U,i}$, and two terms produced by degradation, $Q_{C,i}$ and $Q_{UC,i}$. The constitutive response of the TIMg-UP can be therefore regarded as the parallel combination of the drained (D) response with the reversible (U0) and irreversible (UC) undrained contributions, as illustrated in the one-dimensional layout of the TIMg-UP in Fig. 2a. As a result, the equivalent elastic stiffness $H_{eq,ij}^{(0)}$ of the TIMg-UP corresponds exactly to the inverse of the expression in Eq. (9). The influence of the different contributions {D, U0, UC} on the model response is schematically shown in Fig. 2b, with reference to monotonic and cyclic loading. In particular, the black curve represents the undrained response relating to an initial monotonic loading branch followed by a cyclic stage. In this latter stage, it becomes evident the combined effect of degradation, tending towards a residual fully degraded state, and ratcheting, progressively accumulating irreversible deformations.

Then, the dissipative hydro-mechanical force (Eq. (15)) develops as:

$$\chi^{(C)} = -\frac{\partial \psi}{\partial C} = (1 - U) \bullet \left(\psi_U^{(0)} - \psi_U^{(C)}\right) \tag{18}$$

which is proportional to the difference between the energy content associated with conditions U0 and UC, weighted by the level of drainage through the term 1-U.

By exploiting the orthogonality principle (Ziegler, 1977), the dissipative plastic force can be computed as:

$$\chi_i^{(n)} = -\frac{\partial d}{\partial \dot{q}_i^{(n)}} = \frac{\partial g}{\partial q_i^{(n)}} = Q_i^{(n)} - H_{ij}^{(n)} \bullet q_j^{(n)} \tag{19}$$

where, by comparing Eqs. (14) and (19), it can be inferred that the back force is equal to:

$$c_i^{(n)} = H_{ij}^{(n)} \bullet q_j^{(n)} = \frac{\partial g_2}{\partial q_i^{(n)}} \tag{20}$$

where $g_2 = \sum_{n=1}^{N} H_{ij}^{(n)} \bullet q_j^{(n)} \bullet q_i^{(n)}$ is the part of the Gibbs free energy depending on the plastic deformation only, providing kinematic hardening. In fact, the translation rule for the centre of the n^{th} yield surface derives from Eq. (20), guaranteeing the thermodynamic consistency of deformation processes, such that:

$$\dot{c}_i^{(n)} = \frac{\partial}{\partial t}\left(\frac{\partial g_2}{\partial q_i^{(n)}}\right) = \frac{\partial^2 g_2}{\partial q_i^{(n)} \partial q_j^{(n)}} \bullet \dot{q}_j^{(n)} = \dot{H}_{ij}^{(n)} \bullet \dot{q}_j^{(n)} \tag{21}$$

The derivation of the part concerning ratcheting, $\chi_i^{(R)}$, is instead described in Section 3.4.

3.3. Dissipative response

Introducing Eqs. (14)-(16) into Eq. (12), dissipation assumes the following canonical form, as the sum of the products of conjugates:

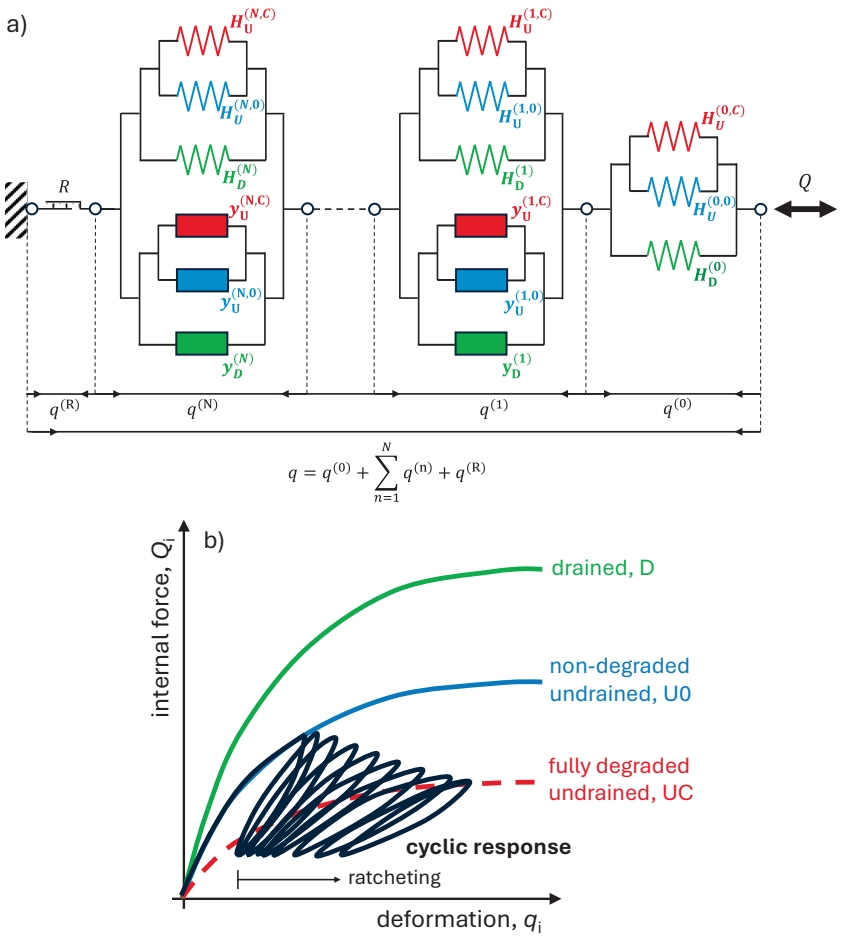


Fig. 2. A) one-dimensional schematic representation of the timg-up and b) associated force–deformation response under monotonic and cyclic loading (the black curve refers to undrained conditions and shows an initial monotonic loading branch followed by a cyclic stage tending to the residual, fully degraded state).

$$\dot{d} = \sum_{n=1}^{N} \chi_i^{(n)} \bullet \dot{q}_i^{(n)} + \chi^{(C)} \bullet \dot{C} + \chi_i^{(R)} \bullet \dot{q}_i^{(R)} \geq 0 \tag{22}$$

Assuming that the plastic flows are associative, dissipation is directly controlled by the shape of the yield surfaces, $y^{(n>0)}$, expressed in the space of the dissipative forces. In fact, dissipation can be derived by a singular version of the Legendre transform, such that:

$$\lambda^{(n)} \bullet y^{(n)} = \chi_i^{(n)} \bullet \dot{q}_i^{(n)} - \dot{d} = 0 \tag{23}$$

which can be conveniently rearranged as:

$$\dot{d} = \lambda^{(n)} \bullet \left(\chi_i^{(n)} \bullet \frac{\partial y^{(n)}}{\partial \chi_i^{(n)}} - y^{(n)} \right) \tag{24}$$

in which $\lambda^{(n)} \geq 0$ is the n^{th} plastic multiplier derived in Section 3.4.

The yield surfaces are taken homothetic to the outermost one, $y^{(N)}$ (Ultimate Surface), as a reasonable assumption verified in previous works (Gorini et al., 2023). The unified analytical model proposed by Gorini (2025) is used to describe the Ultimate Surface of the TIMg-UP, as the load combinations producing failure of a geotechnical system under general patterns (three forces and three moments). The model represents a 6D roto-translated hyper-egg with super-elliptical generatrices applicable to the whole class of geotechnical systems introduced in Section 2. The cartesian equation of the Ultimate Surface is recalled below:

$$\begin{aligned} y^{(N)} = & y_1^{(N)} \bullet y_2^{(N)} - r^{(N)2} \bullet f_{R3}^{(N)2} \bullet \left(1 - \frac{y_3^{(N)}}{f_{q3}^{(N)2} \bullet r^{(N)2}} \right) \\ & \bullet \left(1 + y_{41}^{(N)} \bullet y_{42}^{(N)} - y_{42}^{(N)} \right) = 0 \end{aligned} \tag{25}$$

in which the composed functions $y_i^{(N)}$ are fully defined in Appendix (Eqs. (41)-(48)). In Eqs. (25), (41)-(48), $a_i^{(N)}$ controls the size of the Ultimate Surface in direction i = 1, 2, R1, R2, R3, while $Q_{30}^{(N)}$ and $f_{q3}^{(N)}$ define its width along the Q_3-axis. The ratio $r^{(N)}/b^{(N)}$ identifies the shape of the ultimate locus in the Q_1-Q_2-Q_3 space: as $r^{(N)}/b^{(N)}$ decreases the Ultimate Surface loses its ovoidal shape degenerating into an ellipsoid for $r^{(N)}/b^{(N)} \to 0$. The term t_i is the translation of the Surface in direction i, while the term δ_{ij} produce a rotation of the generalised hyper-egg in the Q_i-Q_j space. Finally, w_i are the exponents of the super-elliptical relations controlling the variability of the ultimate capacity with the external moments Q_{Ri}. For a given geotechnical system, the parameters above can be identified using the procedure in Gorini (2025).

3.4. Incremental response

The incremental form of the TIMg-UP (Eq. (1)) can be obtained by differentiating Eq. (14). In particular, for a linear elastic behaviour within the first yield surface (m = 1 in Eqs. (6)-(7)), the rate of the true force vector reads:

$$\dot{Q}_i = \frac{\partial}{\partial t}\left(\frac{\partial \psi}{\partial q_i^{(0)}}\right) = H_{U,ij}^{(0,0)} \bullet \dot{q}_j^{(0)} + \dot{U} \bullet \left(H_{D,ij}^{(0)} - H_{U,ij}^{(0,0)}\right) \bullet q_j^{(0)} + U \bullet \left(H_{D,ij}^{(0)} - H_{U,ij}^{(0,0)}\right) \bullet \dot{q}_j^{(0)} + \dot{C} \bullet \left(H_{U,ij}^{(0,C)} - H_{U,ij}^{(0,0)}\right) \bullet q_j^{(0)} + C \bullet \left(H_{U,ij}^{(0,C)} - H_{U,ij}^{(0,0)}\right) \bullet \dot{q}_j^{(0)} + \dot{U} \bullet C \bullet \left(H_{U,ij}^{(0,0)} - H_{U,ij}^{(0,C)}\right) \bullet q_j^{(0)} + U \bullet \dot{C} \bullet \left(H_{U,ij}^{(0,0)} - H_{U,ij}^{(0,C)}\right) \bullet q_j^{(0)} + U \bullet C \bullet \left(H_{U,ij}^{(0,0)} - H_{U,ij}^{(0,C)}\right) \bullet \dot{q}_j^{(0)} \quad (26)$$

whose solution requires the definition of the evolution law for the internal variables, as the rate of the elastic deformation vector is equal to $\dot{q}_i^{(0)} = \dot{q}_i - \sum_{n=1}^{N} \dot{q}_i^{(n)} - \dot{q}_i^{(R)}$.

3.4.1. Evolution law for ratcheting

The ratcheting deformation is enforced into the formulation as a constraint, similarly to the technique used in Gorini et al. (2023), according to the following expression:

$$L = \dot{q}_i^{(R)} - \beta \bullet C \bullet \frac{Q_i}{\|Q_i\|} \bullet \frac{\sum_{n=1}^{N} \dot{q}_i^{(n)}}{\|\sum_{n=1}^{N} \dot{q}_i^{(n)}\|} \bullet \sum_{n=1}^{N} \dot{q}_i^{(n)} = \dot{q}_i^{(R)} - f_\beta \bullet \sum_{n=1}^{N} \dot{q}_i^{(n)} = 0 \quad (27)$$

based on which the accumulation of the irreversible ratcheting deformation is a function of the rate of the total plastic deformation through the C-related function f_β. The latter is proportional to the constant β, which in principle requires a trial-and-error calibration against available data on the response of the geotechnical system under numerous cyclic loads. The constraint in Eq. (27) is incorporated in the formulation using the method of the Lagrangian multipliers. Hence, instead of $\dot{d}$, the following dissipation function $\dot{d}^*$ is introduced:

$$\dot{d}^* = \dot{d} + \Lambda \bullet L \quad (28)$$

which is identically equal to $\dot{d}$ by virtue of the condition $L = 0$ (Lagrangian multiplier). In this way, the incremental response can be derived through the unconstrained function $\dot{d}^*$.

3.4.2. Evolution law for U

The drainage factor U is aimed to reproduce the reversible macroscopic effects of the pore water pressure build-up in the foundation soil (see Section 3.1). Its evolution law was derived through a two-step process: 1) identification of the key non-dimensional factors governing the hydro-mechanical response of geotechnical systems; 2) pushover analyses to evaluate the influence of loading rate on the system's macroscopic properties, carried out on a continuum-based soil-foundation model developed in previous works (Lombardi et al., 2024; Lombardi, 2025), and described in Section 4. For conciseness, the results of this process are omitted from the present manuscript, as they are comprehensively documented in Lombardi (2025). It was found that the foundation response is primarily governed by the non-dimensional deformation rate of the geotechnical system Γ, defined as $\|\dot{q}_i\| \bullet B_1 / c_v$ for the translations ($i = 1, 2, 3$) and $\|\dot{q}_i\| \bullet {B_1}^2 / c_v$ for the rotations ($i = $ R1, R2, R3), where c_v is the consolidation coefficient of the participating soil and B_1 the smallest plan dimension of the foundation. In particular, the relationship between U and Γ was established by recognising that, when $C = 0$, the drainage variable can be linked to the initial stiffness of the TIMg-UP through a closed-form expression. In detail, given $\dot{Q}_i$ and $\dot{q}_i$ the drainage variable can be computed from the incremental response in Eq. (26) as $U = \left(H_{ii}^{(0)} - H_{ii}^{(0,U0)}\right) / \left(H_{ii}^{(0,D)} - H_{ii}^{(0,U0)}\right)$. Hence, U was computed for each loading rate, covering the full spectrum from fully drained to undrained conditions.

As a result, the time evolution of U is controlled by the following law:

$$U = \frac{1}{\alpha_U \bullet (\Gamma - \Gamma_0)} \quad (29)$$

based on which U decreases more than linearly as Γ rises. The drainage factor assumes values from 0 to 1 (undrained to drained response, respectively). Eq. (29) is therefore called to satisfy the following conditions: i) $U = 1$ when $\Gamma \le \Gamma_D$ and ii) $U = U^* < 1$ for $\Gamma = \Gamma^* > \Gamma_D$. The input coefficients α_U and Γ_0 can be computed accordingly, and Eq. (29) assumes the following form:

$$U = \frac{U^* \bullet (\Gamma^* - \Gamma_D)}{(1 - U^*) \bullet \Gamma - \Gamma_D + U^* \bullet \Gamma^*} \quad (30)$$

Eq. (30) is illustrated in Fig. 3: it implies a smooth transition from drained to undrained conditions, where the rapidity with which the TIMg-UP approaches impeded drainage can be handled by an appropriate identification of the couple Γ*-U*. The latter represents indeed a threshold between the foundation behaviour characterised by a rapid decrease of U for small increments of Γ (transition region in Fig. 3) and the region in which the response is predominantly controlled by the hydro-mechanical coupling of the soil behaviour (nearly undrained response).

A standardised identification of Γ*-U* implies further investigations beyond the scope of the paper. As a preliminary indication, by virtue of its non-dimensional form, one can refer to the calibration shown in Fig. 3. This was obtained in Lombardi et al. (2024) and Lombardi (2025) as the best fitting of the results of a parametric analysis on a continuum-based numerical model of a shallow foundation resting on saturated soil. As a result, the couple Γ*-U* is equal to 13.9–0.15 and the deformation rate beyond which the response is no longer drained is $\Gamma_D = 6.9$.

3.4.3. Evolution law for C

Degradation of the response can be mainly ascribed to the volumetric-deviatoric coupling of the soil behaviour under non-drained conditions, $U < 1$ (Section 3.1). At the scale of the geotechnical system, it leads to the reduction of the stiffness and resistance of the generalised force–deformation relationship (Lombardi et al., 2024; Lombardi, 2025). In the context of the TIMg-UP framework, this effect is assumed to be related to the accumulation of irreversible deformations occurring in the soil under undrained conditions. This is therefore controlled by the non-dimensional parameter $Mq(t) = \left(\|\sum_{n=1}^{N} q_i^{(n)}(t)\|_{U<1} - \|\sum_{n=1}^{N} q_i^{(n)}(t)\|_{U=1}\right) / B_1$, which is the non-drained aliquot of the plastic deformation vector normalised with respect to the minor length of the foundation in plan.

In the TIMg-UP, degradation is controlled by the damage variable C characterised by the following peculiarities in line with macroscopic hydro-mechanical effects evidenced in previous works (Karamitros et al., 2013a; Karamitros et al., 2013b): C has a full effect under undrained conditions ($U = 0$) whereas its effect vanishes under drained loading ($U = 1$). The damage variable increases under cyclic loading

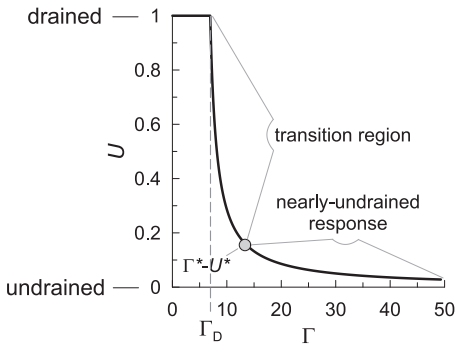


Fig. 3. Example calibration of the evolution law for the drainage factor, U.

with constant amplitude, so the evolution law for C is given in terms of its increment, dC. Moreover, previous works showed that the tendency of the system to degrade reduces with the number of cycles, that is as Mq rises. To account for this effect, for a given Mq, the change in damage is assumed to reduce with the increase of damage accumulation. The following evolution law is proposed accordingly:

$$dC = \left(a_0 + a_1 \bullet Mq + a_2 \bullet Mq^2\right) \bullet \left(1 - b_1 \bullet C - b_2 \bullet C^2\right) \tag{31}$$

where the coefficients a_i and b_i can be computed by imposing the conditions:

$$\begin{cases} dC = 0, C = 0, Mq = Mq_{\min} \\ dC = dC_0, C = 0, Mq = Mq_{\max} \\ \dfrac{\partial(dC)}{\partial Mq} = 0, C = 0, Mq = Mq_{\max} \\ dC = 0, C = 1, Mq = Mq_{\min} \\ \dfrac{\partial(dC)}{\partial C} = 0, C = 1, Mq = Mq_{\max} \end{cases} \tag{32}$$

leading to the quartic surface illustrated in Fig. 4, corresponding to the following expressions of the coefficients:

$$\begin{cases} a_0 = \dfrac{dC_0\left(Mq_{\min}{}^2 - 2Mq_{\min}Mq_{\max}\right)}{\left(Mq_{\max} - Mq_{\min}\right)^2} \\ a_1 = \dfrac{2 \bullet dC_0 \bullet Mq_{\max}}{\left(Mq_{\max} - Mq_{\min}\right)^2} \\ a_2 = -\dfrac{dC_0}{\left(Mq_{\max} - Mq_{\min}\right)^2} \\ b_1 = -2 \\ b_2 = 1 \end{cases} \tag{33}$$

Fig. 4(a) shows the definition of $Mq_{\min}$ and $Mq_{\max}$: degradation occurs starting from the minimum value of the generalised plastic deformation, $Mq_{\min}$, in correspondence of which the rate of degradation is minimum. The rate increases more than linearly as Mq rises and becomes maximum for $Mq \geq Mq_{\max}$. Also, the coupling of Mq and C in Eq. (31) implies that, for a given Mq, the rate of degradation reduces more than linearly as C rises, identifying a residual (fully degraded) condition of the geotechnical system. This, for instance, reproduces cyclic degradation and its evolving nature at constant load amplitudes.

The systematic identification of the parameters for C would require further investigations to standardise degradation effects of geotechnical systems, which will be pursued in subsequent studies. Hence, the shape and size of the surface in Fig. 4 provides a preliminary indication, obtained with a parametric study on the complete soil-foundation model used to calibrate the evolution law for U (Lombardi et al., 2024; Lombardi, 2025).

3.4.4. Evolution law for the n^{th} plastic deformation

The plastic deformation increment vector associated with the n^{th} yield surface is obtained assuming an associated flow rule:

$$\dot{q}_i^{(n)} = \lambda^{(n)} \bullet \frac{\partial y^{(n)}}{\partial \chi_i^{(n)}}, n = 1, 2, \cdots, N \tag{34}$$

in which the gradient of the n^{th} yield surface can be computed by differentiating Eqs. (25), (41)-(48), and the n^{th} plastic multiplier $\lambda^{(n)}$ is determined by invoking the consistency condition, $\dot{y}^{(n)} = 0$. The latter can be written as:

$$\dot{y}^{(n)} = \frac{\partial y^{(n)}}{\partial \chi_i^{(n)}} \bullet \dot{\chi}_i^{(n)} + \frac{\partial y^{(n)}}{\partial q_i^{(n)}} \bullet \dot{q}_i^{(n)} + \frac{\partial y^{(n)}}{\partial U} \bullet \dot{U} + \frac{\partial y^{(n)}}{\partial C} \bullet \dot{C} = 0 \tag{35}$$

which, by virtue of Eqs. (14) and (21), can be developed as:

$$\begin{aligned} \dot{y}^{(n)} &= \frac{\partial y^{(n)}}{\partial \chi_i^{(n)}} \bullet \left(\dot{Q}_i - \dot{c}_i^{(n)}\right) + \frac{\partial y^{(n)}}{\partial q_i^{(n)}} \bullet \dot{q}_i^{(n)} + \frac{\partial y^{(n)}}{\partial U} \bullet \dot{U} + \frac{\partial y^{(n)}}{\partial C} \bullet \dot{C} \\ &= \frac{\partial y^{(n)}}{\partial \chi_i^{(n)}} \bullet \left(\dot{Q}_i - \frac{\partial^2 g_2}{\partial q_i^{(n)} \partial q_j^{(n)}} \bullet \dot{q}_j^{(n)}\right) + \frac{\partial y^{(n)}}{\partial q_i^{(n)}} \bullet \dot{q}_i^{(n)} + \frac{\partial y^{(n)}}{\partial U} \bullet \dot{U} + \frac{\partial y^{(n)}}{\partial C} \bullet \dot{C} \\ &= 0 \end{aligned} \tag{36}$$

By introducing the evolution functions for $\dot{q}_i^{(n)}$ and $\dot{C}$ (Eqs. (34) and (31) into Eq. (36)), the latter becomes:

$$\begin{aligned} \dot{y}^{(n)} &= \frac{\partial y^{(n)}}{\partial \chi_i^{(n)}} \bullet \dot{Q}_i - \frac{\partial y^{(n)}}{\partial \chi_i^{(n)}} \frac{\partial^2 g_2}{\partial q_i^{(n)} \partial q_j^{(n)}} \bullet \lambda^{(n)} \bullet \frac{\partial y^{(n)}}{\partial \chi_j^{(n)}} + \frac{\partial y^{(n)}}{\partial q_i^{(n)}} \bullet \lambda^{(n)} \bullet \frac{\partial y^{(n)}}{\partial \chi_i^{(n)}} + \frac{\partial y^{(n)}}{\partial U} \\ &\quad \bullet \dot{U} + \frac{\partial y^{(n)}}{\partial C} \bullet \dot{C} \\ &= 0 \end{aligned} \tag{37}$$

from which the n^{th} plastic multiplier can be obtained:

$$\lambda^{(n)} = \frac{\frac{\partial y^{(n)}}{\partial \chi_i^{(n)}} \bullet \dot{Q}_i + \frac{\partial y^{(n)}}{\partial U} \bullet \dot{U}}{\frac{\partial y^{(n)}}{\partial \chi_i^{(n)}} \bullet \frac{\partial^2 g_2}{\partial q_i^{(n)} \partial q_j^{(n)}} \bullet \frac{\partial y^{(n)}}{\partial \chi_j^{(n)}} - \frac{\partial y^{(n)}}{\partial q_i^{(n)}} \bullet \frac{\partial y^{(n)}}{\partial \chi_i^{(n)}} - \frac{\partial y^{(n)}}{\partial C} \bullet \dot{C}}, n = 1, 2, \cdots, N \tag{38}$$

in which the term $\partial y^{(n)}\left(\chi_i^{(n)}\right)/\partial q_i^{(n)} = 0$ because the yield functions do not depend on the plastic deformations. Accordingly, the plastic deformation rate is affected by a mixed isotropic-kinematic hardening: the term $\partial y^{(n)}/\partial \chi_i^{(n)} \bullet \partial^2 g_2/\partial q_i^{(n)} \partial q_j^{(n)} \bullet \partial y^{(n)}/\partial \chi_j^{(n)}$ is related to the translation of the yield surfaces in the dissipative force space (kinematic hardening), whilst $\partial y^{(n)}/\partial U \bullet \dot{U}$ is associated with the contraction/expansion of the yield surfaces induced by variations in U (isotropic hardening). The former effect dissipates energy, as prescribed by Eq. (22), whereas the latter is reversible as associated with variations in the drainage factor.

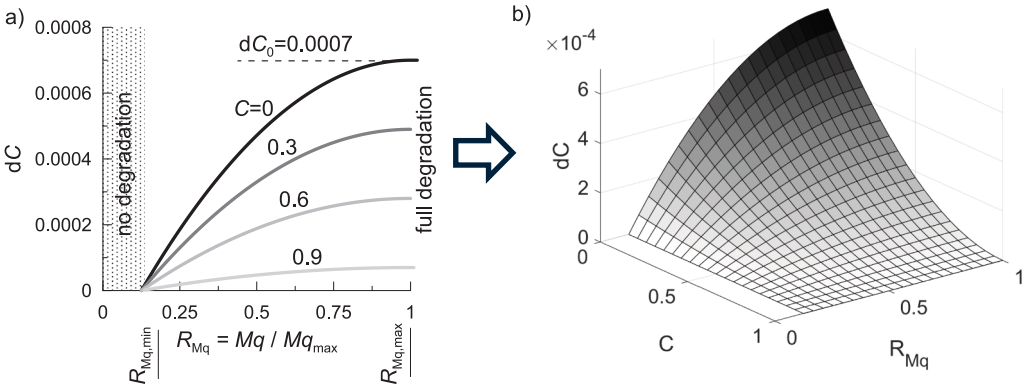


Fig. 4. Evolution law for the rate of the damage variable in the a) 2D and b) 3D space.

3.5. Identification of the TIMg-UP

The calibration of the TIMg-UP for a given geotechnical system requires the quantities in Table 2, that are: i) the ultimate capacity, ii) the initial stiffness and iii) the characterisation of the evolution laws for U and C.

The ultimate capacity is expressed by the Ultimate yield Surface ($y_{D/U}^{(N)}$, Eqs. (25), (41)-(48)). In particular, the latter should be set up under drained ($U = 1$) and undrained ($U = 0$) conditions. This can be achieved by following the procedure proposed by Gorini (2025). The shape, size and orientation of the Ultimate Surface can be indeed calibrated on a few limit conditions of straightforward evaluation, such as the centred bearing capacity, the horizontal limit loads and the maximum external moments that can be transferred to the foundation.

The initial stiffness of the TIMg-UP under drained and undrained conditions is controlled by the tensors $H_{ij,D}^{(0)}$ and $H_{ij,U}^{(0)}$, respectively, enclosed into the nonlinear hyper-elastic law. Many are the available solutions for the initial stiffness of different geotechnical systems; in the undrained case it should be however considered the volumetric incompressibility of the soil skeleton due to the impeded drainage. The parameter m reproduces the dependence of the elastic stiffness on the level of mobilised resistance of the geotechnical system (see Eqs. (6)-(8)). Its systematic calibration will be the objective of future investigations. Notwithstanding, a preliminary indication was obtained through a series of pushover analyses on the soil-foundation model taken as a reference in Sections 3.4.2 and 3.4.3, whose results are omitted for brevity: the value of m reproducing the desired relationship between $H_{ij,D|U}^{(0)}$ and Q_i turned out to range between 1.05 and 1.15. Then, previous works demonstrated that the initial stiffness tensors can be reasonably assumed to be diagonal, as the directional coupling of the TIMg-UP is produced by the prescribed flow rule (Gorini et al., 2023; Gorini and Callisto, 2023).

As a result, the hardening response of the TIMg-UP is controlled by N homothetic yield surfaces. Assuming an extension of the elastic domain equal to 10 % of the Ultimate Surface for both drained and undrained conditions (Gorini et al., 2023; Gorini and Callisto, 2023), the remaining surfaces can be determined by imposing a linear variation of their size. As an example, the initial configuration of the yield surfaces for the shallow foundation analysed in Lombardi et al. (2024) is depicted in Fig. 5, considering $N = 5$.

When the force vector Q_i reaches the n^{th} yield surface, the respective plastic flow is activated and the tangent stiffness matrix H_{ij} is updated. Analogously to the original TIM approach (Gorini et al., 2023; Gorini and Callisto, 2023), the generalised force–deformation constitutive law of the TIMg-UP can, for calibration purposes, be approximated by a hyperbolic relationship, that can be identified focussing on the principal coordinate directions as:

$$Q_i = \frac{q_j}{\left(\frac{1}{H_{ii}^{(0)}} + \frac{q_j}{p_i^{(k)}}\right)}, i = 1, 2, 3, R1, R2, R3 \tag{39}$$

where $p_i^{(k)}$ is the asymptotic value of the force–deformation relationship for the i^{th} degree of freedom. These enhance the flexibility of the TIMg-UP backbone curve, allowing it to capture diverse behaviours typically exhibited by geotechnical systems (Gorini et al., 2023; Gorini and Callisto, 2023; Lombardi et al., 2024). In particular, $p_i^{(k)}$ can be specialised to drained and undrained conditions ($k = D,U$ respectively) to account for the dependence of the tangent stiffness evolution of the macroscopic response of geotechnical systems on drainage conditions (Lombardi et al., 2024). Additional research, which lies beyond the scope of the present work, will be necessary to achieve a generalised calibration procedure of $p_i^{(k)}$ for different systems; as a first step, $p_i^{(k)}$ is calibrated in the following section with reference to a well-documented case study.

Accordingly, the diagonal terms $H_{ii,D/U}^{(n)}$ of each stiffness matrix can be computed to reproduce the relationship in Eq. (39) according to the following expression:

$$H_{ii}^{(n)} = \left(\frac{1}{(dQ_i/dq_i)_{|n}} - \frac{1}{H_{ii}^{(0)}} - \sum_{k=1}^{n-1}\frac{1}{H_{ii}^{(k)}}\right)^{-1}, i = 1,2,3,R1,R2,R3; n = 1,2,\cdots,N \tag{40}$$

where $(dQ_i/dq_i)_{|n}$, obtained by differentiating Eq. (39), represents the system's elastic–plastic tangent stiffness in correspondence of the attainment of the n^{th} yield surface.

Finally, degradation of the TIMg-UP response requires the identification of i) the fully degraded condition of the geotechnical system ($C = 1$), in terms of residual initial stiffness $H_{ij,C}^{(0)}$ and resistance $y_C^{(N)}$, and ii) the parameters {dC_0, Mq_{min}, Mq_{max}} controlling the rate of degradation and the plastic deformation needed to attain the residual state (see Section 3.4). To this end, the fully degraded state can be associated with the collapse of the system driven by the initial gravitational loads transferred to the foundation, $Q_i^{(st)}$, that is, the degraded ultimate capacity in fully undrained conditions ($U = 0$) becomes incompatible with $Q_i^{(st)}$. Accordingly, the initialisation of $y_C^{(N)}$ depends on $Q_i^{(st)}$. Under this assumption, the initial stiffness $H_{ij,C}^{(0)}$ can be simply taken as a small percentage (<1%) of the initial one under the non-degraded, undrained condition, $H_{ij,U}^{(0)}$. As an example, Fig. 5 shows the initial configuration of

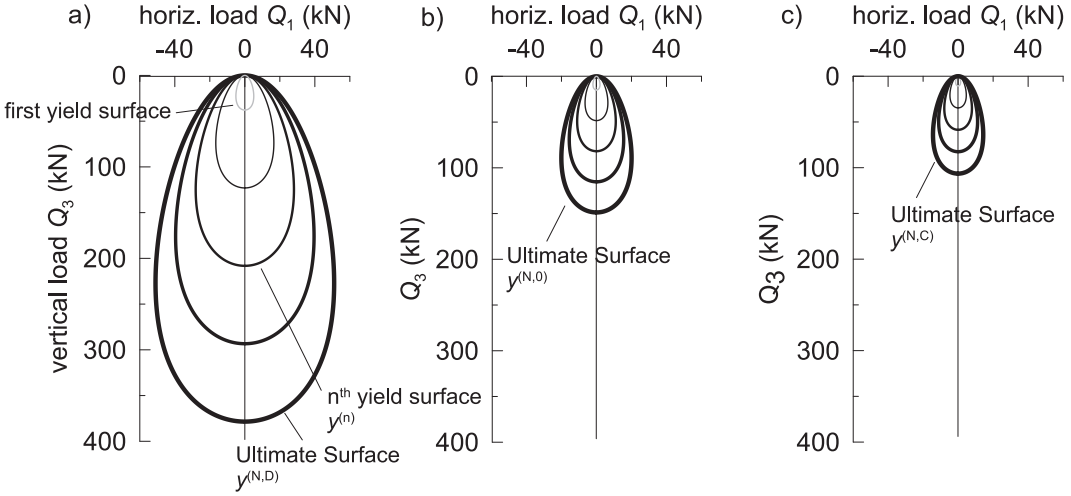


Fig. 5. Initial configuration of the yield surfaces of the TIMg-UP, considering N = 5, for the shallow foundation analysed in Lombardi et al. (2024), corresponding to a) drained, b) non-degraded undrained (U0) and c) fully degraded undrained (UC) conditions.

the yield surfaces for a purely vertical load transferred under static conditions.

The input parameters for the evolution laws of U and C, $\{\Gamma^*, U^*, \Gamma_D\}$ and $\{dC_0, Mq_{max}, Mq_{min}\}$, can be as a first approximation taken as the ones in Section 3.4 for shallow footings, whereas a more systematic identification will be the objective of future studies.

4. THE TIMg-UP AT WORK

The TIMg-UP was implemented as Matlab and C++ constitutive drivers. In the following, its performance is validated against the response of the continuum-based soil-foundation model in Fig. 6, implemented in OpenSees by Lombardi et al. (2024) and Lombardi (2025). The comparison between the two independent models focuses on monotonic and cyclic loading.

The soil-foundation model consists of a square footing of width equal to 1.5 m and thickness of 0.5 m, resting on a sandy soil deposit with small-strain stiffness increasing with depth according to a power law (average shear wave velocity over the vertical extension $V_s = 190$ m/s). The ground water table is coincident with the ground level. The interface at the soil-structure contact is modelled as a thin layer of solid elements with reduced strength parameters interposed between the foundation and the soil (brown layer in Fig. 6). The extension of the soil domain is set to avoid significant boundary effects. By virtue of the symmetry about axis 1, only half of the domain is used to reduce the computation time. The base nodes are fully restrained whilst the nodes along the lateral boundary can move in the vertical direction only.

The soil domain is discretised through 7680 8-nodes hexahedral SSPbrickUP-type elements (McGann et al., 2015). The soil behaviour is described by the pressure-dependent multi-yield surface model developed by Yang et al., 2003, denoted as PDMY. It is an elastic–plastic constitutive law with kinematic hardening providing a piecewise linear stress–strain relationship largely used for coarse-grained soils. The model parameters were calibrated to exhibit a substantially contractant behaviour (see Lombardi et al., 2024, and Lombardi, 2025). The foundation is instead modelled as 4-noded ShellMITC4-type quadrilateral elements (Dvorkin and Bathe, 1984) exhibiting a linear viscoelastic behaviour. The numerical analyses were carried out using domain decomposition through the interpreter OpenSeesSP (McKenna and Fenves, 2008), in conjunction with the supercomputing resources of the Texas Advanced Computing Centre (TACC, Rathje et al., 2017).

As a preliminary step, the TIMg-UP was calibrated following the procedure outlined in Section 3.5, complemented by a series of pushover analyses carried out on the model of Fig. 4. These analyses were employed to calibrate $p_i^{(k)}$ and the input parameters for the evolution laws for U and C; the corresponding results are omitted for brevity. A comprehensive description of the test campaign carried out on the continuum-based soil-foundation model is reported in Lombardi (2025). Table 3 reports the values of the stiffness and strength parameters of the TIMg-UP, whilst Table 4 summarizes the values of the parameters that govern the evolution laws for the drainage and damage variables.

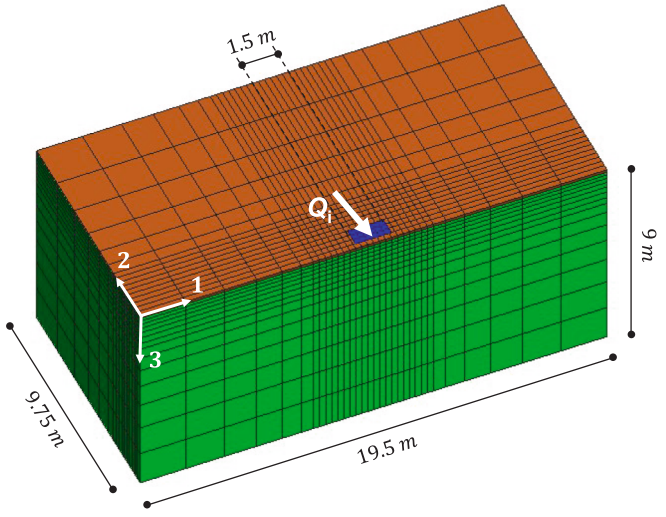


Fig. 6. Reference soil-shallow foundation model (reproduced from Lombardi et al., 2024).

4.1. Monotonic response

The TIMg-UP is initially tested under monotonic conditions. A series of pushover analyses were carried out following different load paths. Each analysis included the preliminary application (Stage 1) under drained conditions of a vertical load equal to 30 % of the bearing capacity in compression of the footing, representing a service load transferred by the superstructure. It was kept constant during the subsequent stage, No. 2, involving a monotonic increase of additional load components.

Fig. 7 illustrates the TIMg-UP response in the case of the separate application of an increasing vertical load or moment around axis 2 in Stage 2. The performance is tested against the results of the reference complete model of Fig. 6, in which deformations of the foundation refer to its central node. The analyses were carried out considering a different level of drainage of the pore water, spanning from fully drained to undrained conditions. In the complete model, this was achieved by changing the soil permeability and the load velocity, avoiding concomitantly the occurrence of significant inertial effects; instead, the TIMg-UP was forced to exhibit a prescribed drainage level by simply setting a constant value for U, from 0 to 1, maintaining the evolution of C as prescribed by Eqs. (39)-(41). The remaining input parameters of the TIMg-UP were calibrated according to the procedure discussed in Section 3.5 and with reference to the evolution laws for U and C relating to the foundation at hand, illustrated in Figs. 3 and 4.

For both loading paths (Figs. 7a and 7b), the TIMg-UP simulates satisfactorily the results of the complete model. An undrained response reduces the stiffness and resistance of the soil-foundation system. The detrimental effect appears substantial when the foundation is loaded in the vertical direction, whereas it becomes less significant, despite not negligible, on the rotational response. This can be attributed to the fact that, compared to a purely vertical deformation mode, the rotational response involves a smaller volume of soil localised in proximity of the foundation edge, leading to a response that is less sensitive to the generation of the excess pore water pressure. The partly drained response of

Table 2
Input parameters of the TIMg-UP.

	Parameter	Description
Drained	$H_{ij,D}^{(0)}$	Initial stiffness matrix
	$p_i^{(D)}$	Asymptote of the backbone curves along directions $i = 1,2,3,R1,R2,R3$
	m	Stress-dependent coefficient of the nonlinear elastic stiffness
	$y_D^{(N)}$	Ultimate yield surface
Non-degraded undrained	$H_{ij,U}^{(0)}$	Initial stiffness matrix
	$p_i^{(U)}$	Asymptote of the backbone curves along directions $i = 1,2,3,R1,R2,R3$
	$y_U^{(N)}$	Ultimate yield surface
	Γ_D	Drained-threshold non-dimensional deformation rate
	Γ^*	Scrutiny non-dimensional deformation rate
	U^*	Scrutiny drainage level
Fully degraded undrained response	$y_C^{(N)}$	Ultimate yield surface
	dC_0	Initial non-dimensional degradation rate
	Mq_{min}	Non-dimensional plastic deformation for degradation triggering
	Mq_{max}	Non-dimensional plastic deformation under fully degraded conditions

Table 3
Stiffness and strength parameters of the TIMg-UP calibrated for the reference case.

	$H_{11}^{(0)}$	$H_{33}^{(0)}$	$H_{R2R2}^{(0)}$	$p_1^{(k)}$	$p_3^{(k)}$	$p_{R2}^{(k)}$	m	$Q_3^{(+)}$	$a_1^{(N)}$	$a_{r2}^{(N)}$	$r^{(N)}/b^{(N)}$
drainage cond.	(kN/m)	(kNm)	(kN/m)	(kN)	(kN)	(kNm)	(−)	(kN)	(−)	(−)	(−)
D	1.47e5	1.16e5	5.26e4	70.1	1050	50.4	1.17	378.5	250.0	170.0	0.2
U	1.81e5	9.87e4	5.82e4	21.4	224.3	17.9	1.05	148.8	98.3	66.8	0.2
C	1.81e5	9.87e4	5.82e4	21.4	224.3	17.9	1.05	106.5	70.3	47.8	0.2

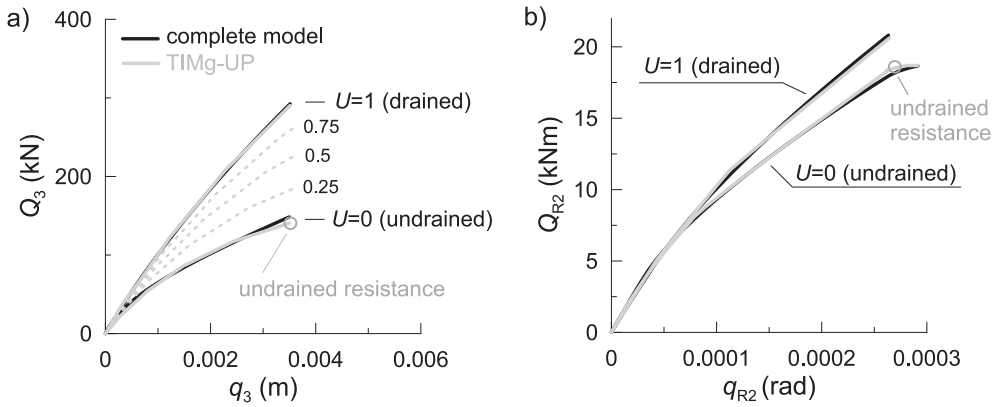


Fig. 7. Comparison between the response of the continuum soil-foundation model (black lines) and the TIMg-UP (grey lines): application of a) a vertical force and b) an external moment, for different drainage levels.

the TIMg-UP ($0 < U < 1$ in Fig. 7a) leads to a progressive evolution of the macroscopic properties of the geotechnical system. It is worth noticing the enormous computational gain obtained with the proposed approach: a single pushover analysis on the macroelement takes about 3 s on a common laptop, instead of 6 h needed to run the complete model using parallel computing on supercomputing resources.

The combined horizontal-rotational response of the TIMg-UP is illustrated in Fig. 8. With respect to purely uniaxial load patterns (dashed lines in the figure), the directional coupling of the macroelement response appears fundamental for a proper assessment of the multiaxial stiffness and resistance of the geotechnical system. The performance is moreover affected by the level of drainage of the pore water in the participating soil. In fact, impeded drainage causes a significant reduction of the resistance and an increment of the macroscopic rotational stiffness. The latter effect is less evident on the horizontal response as it is less sensitive to the pore water pressure build-up.

4.2. Cyclic response

The level of drainage and degradation in the TIMg-UP affects the response under cyclic loading as well. This is first highlighted in Fig. 9,

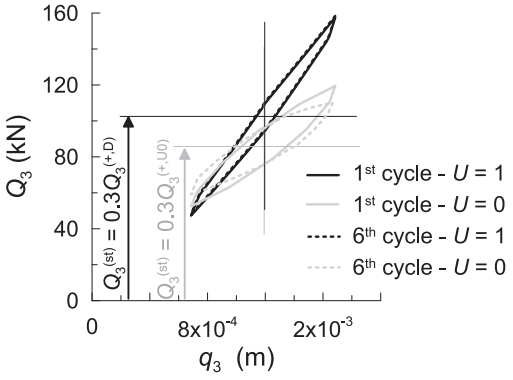


Fig. 9. Effect of the cyclic evolution of the damage variable C: vertical response of the TIMg-UP under cyclic loading at the first and sixth cycle, under drained and undrained conditions.

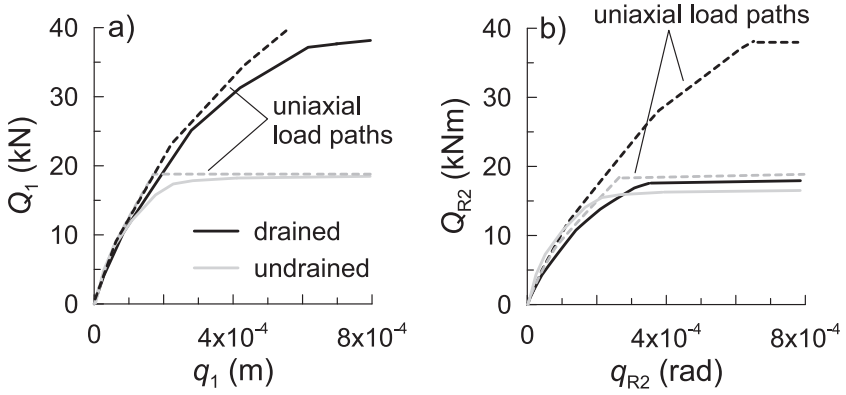


Fig. 8. Response of the TIMg-UP perturbed by an increasing horizontal load, Q_1, and an external moment $Q_{R2} = Q_1 \times 0.5$ m, at a constant $Q_3 = 0.3Q_3^{(+)}$, under drained (U = 1) and undrained (U = 0) conditions. Dashed lines refer to as the corresponding uniaxial loading paths, i.e., increasing Q_1 or Q_{R2} separately.

showing the macroelement response in displacement-controlled cyclic simulations where a harmonic vertical load oscillates around its initial value, taken as 30 % of the bearing capacity in compression under drained and undrained conditions, $Q_3^{(+,D)}$ and $Q_3^{(+,U0)}$ respectively.

It can be inferred that, for a given amplitude of the applied deformation q_3, the undrained response is characterised by higher energy dissipation (larger hysteresis loops) compared to drained conditions because the same vertical displacement q_3 corresponds to much higher level of mobilised resistance in the former case. In fact, four plastic flows are activated in the undrained response instead of three in the drained case. The drained response shows, as expected, a stable hysteresis loop not depending on the number of cycles. On the contrary the undrained response is unstable because of degradation, which activates when $U < 1$. This produces a progressive decrement of the tangent stiffness and resistance of the macroelement as plastic deformations accumulate, resulting in an increasing rotation of the force–deformation loop with the number of cycles.

As an assessment of the sensitivity of the TIMg-UP response to the initialisation of dC_0, the undrained analyses above ($U = 0$) were carried out again for 20 cycles considering a large variability of the parameter, keeping the thresholds $Mq_{\min}$ and $Mq_{\max}$ unchanged to isolate the effect of the degradation rate. With respect to the reference value $dC_0 = 7\text{x}10^{-4}$, the parameter was varied by a factor of $\pm$ 10. The results in Fig. 10a show the evolution of the ratio $r_{H33}=H_{33}^{(sec)}/H_{33}^{(sec)}(C = 0)$ between the secant vertical stiffness of the TIMg-UP and that of the non-degraded undrained response, related to the number of cycles, N_{cyc}. As expected, larger values of dC_0 reduces the number of cycles required to attain the residual, fully degraded condition. However, for the configuration adopted in Table 4, changes in dC_0 moderately affect the secant stiffness with variations not exceeding 10 %.

Fig. 10b depicts the resulting force–deformation relationships at the tenth loading cycle. A moderate reduction in the secant stiffness with increasing dC_0 is observed, while the variation in the hysteresis loop area (dissipated energy) is negligible. Therefore, although a broader study is needed to generalise the calibration of the parameters controlling the evolution of C (Table 4), the results in Fig. 10 indicate that, for a given calibration of the TIMg-UP, the cyclic response is not highly sensitive to the variability of the initial degradation rate.

The peculiar TIMg-UP's features pointed out above are now compared with the results of the complete soil-shallow foundation model of Fig. 6. Starting from the application of a vertical load equal to $0.3Q_3^{(+,D|U)}$, kept constant in time, both models are perturbed by a harmonic load with increasing amplitude in the horizontal and rotational global degree of freedom of the footing, Q_1 and Q_{R2} respectively. At the last cycle the load attains the ultimate capacity of the geotechnical system, evaluated through previous monotonic tests omitted for brevity. The cyclic perturbation is characterised by a sufficiently large period, equal to 10 s, to avoid the occurrence of inertial effects. The cyclic stage was carried out considering fully drained or undrained conditions for the soil, reproduced according to the procedures discussed in Section 4.1.

Table 4
Parameters governing the evolution laws of U and C, calibrated for the reference case (Fig. 4).

Γ_D	Γ^*	U^*	Mq_{min}	Mq_{max}	dC_0
6.94	13.9	0.15	1.0e-4	8.0e-4	7.0e-4

The resulting force–deformation and moment-rotation relationships of the geotechnical system are shown in Figs. 11 and 12. The TIMg-UP simulates quite satisfactorily the translational and rotational response of the foundation in the continuum-based model requiring a drastically lower computational effort: a sole cyclic analysis on the TIMg-UP requires 12 s on a laptop instead of 36 h using the TACC supercomputing resources (Rathje et al., 2017) with domain decomposition. For a given mobilised resistance, the undrained response is featured by an increased secant stiffness at the macro-scale compared to the drained one, as the impeded drainage of the pore water increases the *meso*-scale volumetric stiffness of the soil. Nonetheless, the undrained capacity is much lower because of the reduced effective stresses in the soil participating to the foundation response.

The considerations above hold for the rotational response as well. However, the proposed calibration of the TIMg-UP leads to some discrepancies with respect to the response of the complete soil-foundation model. Indeed, albeit the good reproduction of the hysteresis loops, the TIMg-UP underestimates (15 % and 4 % for the drained and undrained cases, respectively) the secant rotational stiffness at failure (last cycle). This can be mainly ascribed to the hyperbolic model adopted for the evolution of the tangent stiffness of the macroelement with the level of the mobilised resistance, prescribed by Eqs. (39)-(40). This aspect should be better specialised through the aid of further investigations on the rotational response, that are beyond the scope of the paper.

4.3. Seismic loading

This section is finally devoted to show the role of the coupled hydro-mechanical behaviour of the foundation soil on the performance of the TIMg-UP subjected to a variable transient loading. The macroelement calibration considered by far is also adopted in the following. The TIMg-UP is perturbed by the horizontal component of a natural seismic record relating to the L'Aquila earthquake (Italy, 2009). The record, shown in Fig. 13a, was selected from the web-based PEER ground motion database (record ID: RSN 4477, website: https://ngawest2.berkeley.edu/) and the respective amplitudes were scaled down to highlight the system response in a wide range of deformation levels.

The seismic motion above was applied to the macroelement as a displacement time-history, computing the resulting force components. The force–deformation relationship of the macroelement is shown in Fig. 14, comparing the drained response (U set equal to 1 throughout the

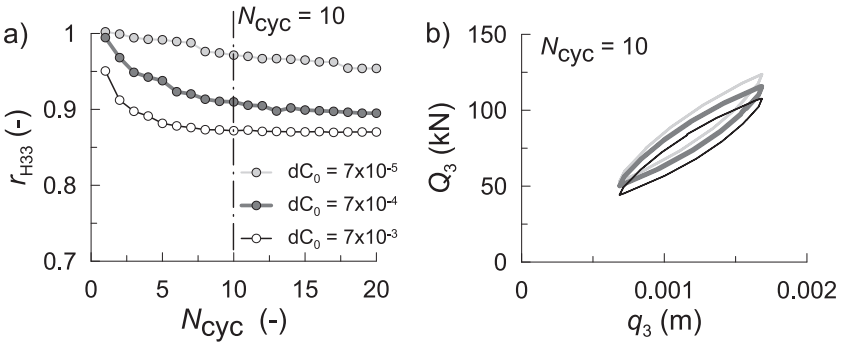


Fig. 10. A) Undrained, vertical secant stiffness of the TIMg-UP, normalised to the undrained non-degraded condition (C = 0), plotted as a function of the number of cycles, for different values of dC$_0$; b) associated force–deformation cycles in correspondence of the tenth cycle.

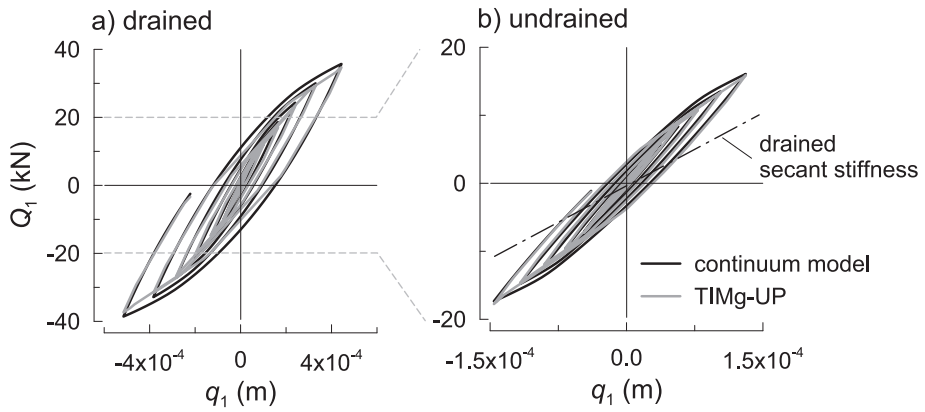


Fig. 11. TIMg-UP vs continuum-based soil-foundation model: cyclic response produced by an increasing horizontal load, Q_1, at a constant $Q_3 = 0.3Q_3^{(+)}$, under a) drained and b) undrained conditions.

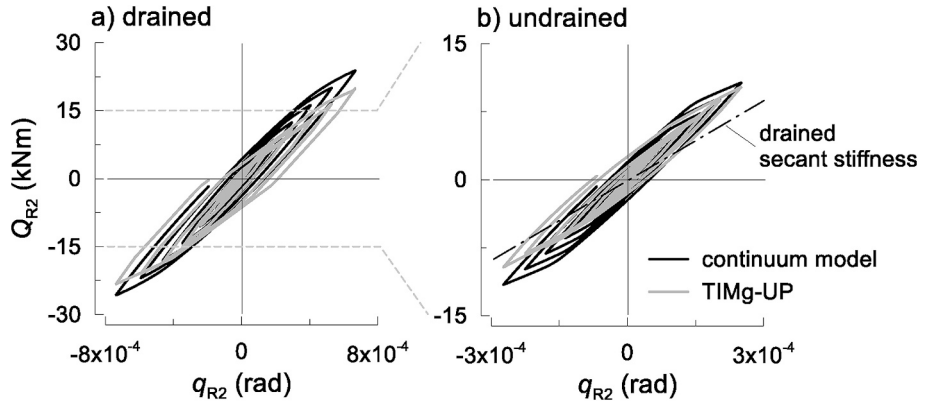


Fig. 12. TIMg-UP vs continuum-based soil-foundation model: cyclic response produced by an increasing external moment Q_{R2}, at a constant $Q_3 = 0.3Q_3^{(+)}$, under a) drained and b) undrained conditions.

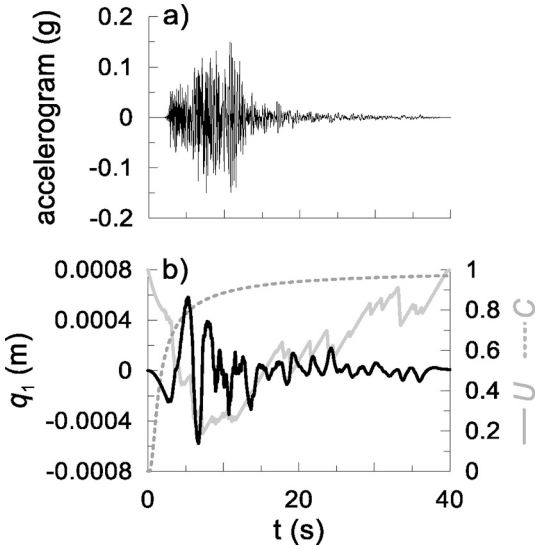


Fig. 13. A) Selected seismic record and b) corresponding time evolutions of the displacement, drainage and degradation variables.

analysis, Fig. 14a), the undrained one ($U = 0$, Fig. 14c) and the response in which U varies in time according to the respective evolution law (Fig. 14b). In the latter two cases, the hydro-mechanical coupling produces cyclic degradation because of the activation of the damage variable C. For the seismic scenario at hand, the effective time evolutions of U and C are represented in Fig. 13.

The fully drained analysis is exactly the response that can be obtained using the previous macroelement version, TIM-G, without hydro-mechanical coupling (Gorini, 2025). The fully undrained response of the TIMg-UP differs instead from the one that can be simulated with the TIM-G (calibrated on the system's undrained resistance) for the effects relating to cyclic degradation. From Figs. 13 and 14 it is evident that, even under seismic loading, the effective response is different from that obtained under drained and undrained conditions. In fact, the effective drainage factor is always lower than 1 during the seismic motion but never reaches a purely undrained state ($U = 0$). This leads to the force–deformation response in Fig. 14c, showing an intermediate behaviour between the limit conditions (Figs. 14a,c). Accordingly, a merely drained/undrained assumption, commonly used in time-domain analysis employing macroelements, can lead to a substantially erroneous assessment of the deformation demand for the foundation elements as well as of the dynamic forces in the geotechnical system, which affect in turn the deformation and ductility demand for the members of the superstructure.

5. Conclusions

The proposed macroelement, TIMg-UP, can be regarded as a useful design tool for the inclusion of soil-structure interaction effects in the analysis of bridges and buildings. By virtue of a minimum computational burden and an efficient management of the numerical model, the TIMg-UP simulates salient aspects of soil-structure interaction. More in detail,

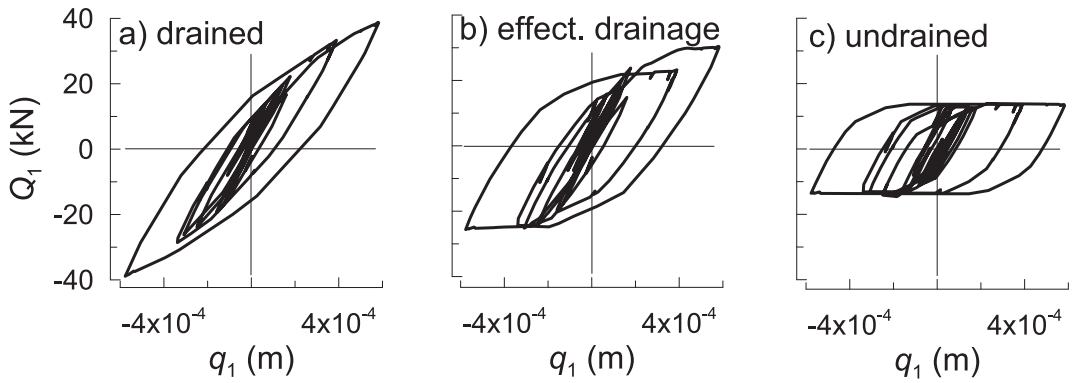


Fig. 14. Horizontal force–deformation response of the TIMg-UP to seismic loading: comparison between a) the drained, b) the variable drainage and c) the undrained responses.

the TIMg-UP extends the TIM-G approach (Gorini, 2025) by relating a nonlinear, fully coupled 6D response to the hydro-mechanical coupling in the foundation soils. These multi-physics effects are modelled according to a hyper-elastic and hyper-plastic formulation with mixed hardening producing consistent deformation processes with the Laws of Thermodynamics.

The TIMg-UP is coded as a multiaxial material lumping the response of the whole soil-foundation system. It is available for Matlab and OpenSees and can be employed in many applications, spanning from specific cases to territorial assessments. The macroelement was seen to simulate efficiently the hydro-mechanical response of a reference geotechnical system, described by a more demanding and advanced numerical technique, that was taken as a reference for comparison. The role of the coupled hydro-mechanical soil behaviour on the system performance was highlighted: it is a function of the drainage level of the pore water, that depends in turn on the frequency of the external perturbation. Dynamic loading produces a time-dependent evolution of the stiffness and resistance of a geotechnical system, as an effect neglected by existing macroelements that can compromise the evaluation of foundation and superstructure members.

Although its standardised application requires further investigations, the TIMg-UP formulation can potentially open to the extensive assessment of structures against natural hazards considering the distinct multi-physics nature of the mechanical soil behaviour, of primary interest, for instance, for seismic analysis of offshore structures or in the presence of liquefiable soils and multi-hazard scenarios.

CRediT authorship contribution statement

Davide Noè Gorini: Writing – review & editing, Writing – original draft, Validation, Supervision, Project administration, Methodology, Investigation, Formal analysis, Data curation, Conceptualization. **Giuseppe Lombardi:** Writing – review & editing, Visualization, Validation, Investigation, Conceptualization. **Luigi Callisto:** Writing – review & editing, Supervision, Conceptualization.

Declaration of competing interest

The authors declare that they have no known competing financial interests or personal relationships that could have appeared to influence the work reported in this paper.

Acknowledgments

None

Appendix

The composed functions of the generalised Ultimate Surface in Eq. (25) were fully derived in Gorini (2025) and are recalled below:

$$y_1^{(N)} = \frac{[\cos(\delta_{31}) \bullet \cos(\delta_{1R2}) \bullet (Q_1 - t_1) - \sin(\delta_{31}) \bullet (Q_3 - t_3) - \sin(\delta_{1R2}) \bullet (Q_{R2} - t_{R2})]^2}{a_1^{(N)2}} + \frac{[\sin(\delta_{1R2}) \bullet (Q_1 - t_1) - \sin(\delta_{3R2}) \bullet (Q_3 - t_3) + \cos(\delta_{3R2}) \bullet \cos(\delta_{1R2}) \bullet (Q_{R2} - t_{R2})]^2}{a_{R2}^{(N)2}} \tag{41}$$

$$y_2^{(N)} = \left\{ b^{(N)} - r^{(N)} \bullet \left[\frac{\sin(\delta_{31}) \bullet Q_1 + \cos(\delta_{31}) \bullet \cos(\delta_{3R2}) \bullet Q_3 + \sin(\delta_{3R2}) \bullet Q_{R2}}{f_{R3}^{(N)} \bullet f_{q3}^{(N)} \bullet f_{FR2}^{(N)} \bullet r^{(N)}} - \frac{Q_{30}^{(N)} + b^{(N)} \bullet f_{q3}^{(N)}}{f_{q3}^{(N)} \bullet r^{(N)}} \right] \right\}^2 \tag{42}$$

$$y_3^{(N)} = \left[\frac{\sin(\delta_{31}) \bullet Q_1 + \cos(\delta_{31}) \bullet \cos(\delta_{3R2}) \bullet Q_3 + \sin(\delta_{3R2}) \bullet Q_{R2}}{f_{R3}^{(N)} \bullet f_{FR2}^{(N)}} - - Q_{30}^{(N)} - b^{(N)} \bullet f_{q3}^{(N)} \right]^2 \tag{43}$$

$$y_{41}^{(N)} = \left\{ 1 + \left[\frac{a_1^{(N)}}{a_2^{(N)}} \bullet \frac{\cos(\delta_{2R3}) \bullet \cos(\delta_{2R1}) \bullet Q_2 - \sin(\delta_{2R1}) \bullet Q_{R1} - \sin(\delta_{2R3}) \bullet Q_{R3}}{\cos(\delta_{31}) \bullet \cos(\delta_{1R2}) \bullet Q_1 - \sin(\delta_{31}) \bullet Q_3 - \sin(\delta_{1R2}) \bullet Q_{R2}} \right]^2 \right\}^{-1} \left\{ 1 + \left[\frac{a_1^{(N)}}{a_{R2}^{(N)}} \bullet \frac{\sin(\delta_{1R2}) \bullet Q_1 - \sin(\delta_{3R2}) \bullet Q_3 - \cos(\delta_{3R2}) \bullet \cos(\delta_{1R2}) \bullet Q_{R3}}{\cos(\delta_{31}) \bullet \cos(\delta_{1R2}) \bullet Q_1 - \sin(\delta_{31}) \bullet Q_3 - \sin(\delta_{1R2}) \bullet Q_{R2}} \right]^2 \right\}^{-1} \tag{44}$$

$$y_{42}^{(N)} = f_{FR2}^{(N)2} = \left\{ 1 + [\![\frac{a_1^{(N)}}{a_{R1}^{(N)}} \bullet \frac{\sin(\delta_{2R1}) \bullet Q_2 + \cos(\delta_{2R1}) \bullet Q_{R1}}{\cos(\delta_{31}) \bullet \cos(\delta_{1R2}) \bullet Q_1 - \sin(\delta_{31}) \bullet Q_3 - \sin(\delta_{1R2}) \bullet Q_{R2}} \left[1 + \left(\frac{a_1^{(N)}}{a_{R2}^{(N)}} \bullet \frac{\sin(\delta_{1R2}) \bullet Q_1 - \sin(\delta_{3R2}) \bullet Q_3 - \cos(\delta_{3R2}) \bullet \cos(\delta_{1R2}) \bullet Q_{R3}}{\cos(\delta_{31}) \bullet \cos(\delta_{1R2}) \bullet Q_1 - \sin(\delta_{31}) \bullet Q_3 - \sin(\delta_{1R2}) \bullet Q_{R2}} \right)^2 \right]^{-0.5 \; w_{h3R1R2}}]\!] \right\}^{\frac{2}{w_{h3R1R2}}} = \left[1 + \left(\frac{f_{FR2,N}^{(N)}}{f_{FR2,D}^{(N)}} \right)^{w_{h3R1R2}} \right]^{\frac{1}{w_{h3R1R2}}} \tag{45}$$

$$f_{FR2,N}^{(N)} = \frac{a_1^{(N)}}{a_{R1}^{(N)}} \bullet \frac{\sin(\delta_{2R1}) \bullet Q_2 + \cos(\delta_{2R1}) \bullet Q_{R1}}{\cos(\delta_{31}) \bullet \cos(\delta_{1R2}) \bullet Q_1 - \sin(\delta_{31}) \bullet Q_3 - \sin(\delta_{1R2}) \bullet Q_{R2}} \tag{46}$$

$$f_{FR2,D}^{(N)} = \left[1 + \left(\frac{a_1^{(N)}}{a_{R2}^{(N)}} \bullet \frac{\sin(\delta_{1R2}) \bullet Q_1 - \sin(\delta_{3R2}) \bullet Q_3 - \cos(\delta_{3R2}) \bullet \cos(\delta_{1R2}) \bullet Q_{R3}}{\cos(\delta_{31}) \bullet \cos(\delta_{1R2}) \bullet Q_1 - \sin(\delta_{31}) \bullet Q_3 - \sin(\delta_{1R2}) \bullet Q_{R2}} \right)^2 \right]^{0.5} \tag{47}$$

$$f_{R3} = \left[1 - \left(\frac{\overline{Q}_{R3}}{a_{R3}^{(N)}} \right)^{w_{h3RhR3}} \right]^{\frac{1}{w_{h3RhR3}}} \tag{48}$$

Data availability

Data will be made available on request.

References

Bazaios, K.N., Papadimitriou, A.G., Bouckovalas, G.D., Tsiapas, Y.Z., 2023. Effect of structural inertia on liquefaction-induced settlements of shallow foundations. Soil Dyn. Earthq. Eng. 164, 107546.

Casablanca, O., Biondi, G., Cascone, E., 2023. Bearing capacity of shallow foundations accounting for seismic excess pore pressures. Soil Dyn. Earthq. Eng. 173, 108090.

Cascone, E., Bouckovalas, G., 1998. Seismic bearing capacity of footings on saturated sand with a clay cap. Balkema Publishers.

Collins, I. F., & Houlsby, G. T. (1997). Application of thermomechanical principles to the modelling of geotechnical materials. Proceedings of the Royal Society of London. Series A: Mathematical, Physical and Engineering Sciences, 453(1964), 1975-2001.

Dashti, S., Bray, J.D., Pestana, J.M., Riemer, M., Wilson, D., 2010. Centrifuge testing to evaluate and mitigate liquefaction-induced building settlement mechanisms. J. Geotech. Geoenviron. Eng. 136 (7), 918–929.

Dvorkin, E.N., Bathe, K.J., 1984. A continuum mechanics based four-node shell element for general non-linear analysis. Engineering computations 1 (1), 77–88.

Einav, I., Cassidy, M.J., 2005. A framework for modelling rigid footing behaviour based on energy principles. Comput. Geotech. 32 (7), 491–504.

Elgamal, A., Yan, L., Yang, Z., Conte, J.P., 2008. Three-dimensional seismic response of Humboldt bay bridge-foundation ground system. Journal of Structural Engineering (ASCE) 134 (7), 1165–1176.

Flessati, L., di Prisco, C., Callea, F., 2021. Numerical and theoretical analyses of settlements of strip shallow foundations on normally consolidated clays under partially drained conditions. Géotechnique 71 (12), 1114–1134.

Franchin, P., Baltzopoulos, G., Biondini, F., Callisto, L., Capacci, L., Carbonari, S., Dall'Asta, A., Flora, A., Gorini, D.N., Iervolino, I., Marchi, A., Noto, F., Perrone, G., 2023. Seismic reliability of italian code-conforming bridges. Earthq. Eng. Struct. Dyn. 52 (14), 4442–4465.

Gallese, D., Gorini, D.N., Callisto, L., 2023. Seismic design of integral abutment bridges using nonlinear static analysis of soil-structure numerical models. Geotechnique. https://doi.org/10.1680/jgeot.22.00229.

Gorini, D.N., 2025. A unified thermodynamic-based macroelement for geotechnical systems. Comput. Geotech. 179, 106965. https://doi.org/10.1016/j.compgeo.2024.106965.

Gorini, D.N., Callisto, L., 2020. A coupled study of soil-abutment-superstructure interaction. Springer Lecture Notes in Civil Engineering "Geotechnical Research for Land Protection and Development" (CNRIG2019), 40, 565–574.

Gorini, D.N., Callisto, L., 2023. A multiaxial inertial macroelement for deep foundations. Comput. Geotech. 155, 105222.

Gorini, D.N., Callisto, L., Whittle, A.J., 2022. An inertial macroelement for bridge abutments. Geotechnique 72 (3), 247–259.

Gorini, D.N., Callisto, L., Whittle, A.J., Sessa, S., 2023. A multiaxial inertial macroelement for bridge abutments. Int. J. Numer. Anal. Meth. Geomech. 47 (5), 793–816.

Houlsby, G.T., Puzrin, A., 2000a. A thermomechanical framework for constitutive models for rate-independent dissipative materials. Int. J. Plast 16 (9), 1017–1047.

Houlsby, G.T., Puzrin, A.M., 2000b. An approach to plasticity based on generalised thermodynamics. In: Constitutive Modelling of Granular Materials. Berlin, Heidelberg, Springer, Berlin Heidelberg, pp. 319–331.

Houlsby, G.T., Puzrin, A.M., 2006. Principles of hyperplasticity. Springer, Berlin.

Houlsby, G.T., Abadie, C., Beuckelaers, W., Byrne, B., 2017. A model for nonlinear hysteretic and ratcheting behaviour. Int. J. Solids Struct. 120, 67–80.

Karamitros, D.K., Bouckovalas, G.D., Chaloulos, Y.K., Andrianopoulos, K.I., 2013a. Numerical analysis of liquefaction-induced bearing capacity degradation of shallow foundations on a two-layered soil profile. Soil Dyn. Earthq. Eng. 44, 90–101.

Karamitros, D.K., Bouckovalas, G.D., Chaloulos, Y.K., 2013b. Insight into the seismic liquefaction performance of shallow foundations. J. Geotech. Geoenviron. Eng. 139 (4), 599–607.

Kotsoglou, K., Pantazopoulou, S., 2007. Bridge-embankment interaction under transverse ground excitation. Earthq. Eng. Struct. Dyn. 36 (12), 1719–1740.

Kotsoglou, A., Pantazopoulou, S., 2009. Assessment and modeling of embankment participation in the seismic response of integral abutment bridges. Bull. Earthq. Eng. 7, 343–361.

Le Pape, Y., Sieffert, J.G., 2001. Application of thermodynamics to the global modelling of shallow foundations on frictional material. Int. J. Numer. Anal. Meth. Geomech. 25 (14), 1377–1408.

Liu, L., Dobry, R., 1997. Seismic response of shallow foundation on liquefiable sand. J. Geotech. Geoenviron. Eng. 123 (6), 557–567.

Lombardi, G. (2025). Identification, implementation, and validation of a macro-element for the cyclic response of shallow foundations in saturated soils. Phd thesis.

Lombardi, G., Gorini, D.N., Callisto, L., 2024. On the dynamic response of shallow foundations in saturated soils. Japanese Geotechnical Society Special Publication 10 (55), 2084–2089.

McGann, C.R., Arduino, P., Mackenzie-Helnwein, P., 2015. A stabilized single-point finite element formulation for three-dimensional dynamic analysis of saturated soils. Computers and Geotechnics 66, 126–141.

McKenna, F., & Fenves, G.L. (2008). Using the OpenSees interpreter on parallel computers. *Network for earthquake engineering simulations*.

Nguyen-Sy, L., Nguyen-Sy, L., 2005. The theoretical modelling of circular shallow foundation for offshore wind turbines. Oxford University, UK). Doctoral dissertation.

Nova, R., Montrasio, L., 1991. Settlements of shallow foundations on sand. Géotechnique 41 (2), 243–256.

Peccin da Silva, A., Diambra, A., Karamitros, D., Chow, S.H., 2023. A Cyclic Macro-Element Framework for Consolidation-Dependent Three-Dimensional Capacity of Plate Anchors. Journal of Marine Science and Engineering.

Prevost, J.H., 1978. Plasticity theory for soil stress-strain behavior. URL J .Eng. Mech. Div. 104 (5), 1177–1194. https://cedb.asce.org/CEDBsearch/record.jsp?dockey=0008331.

Rahmani, A., Taiebat, M., Liam Finn, W.D., 2014. Nonlinear dynamic analysis of Meloland Road Overpass using three-dimensional continuum modeling approach. Soil Dyn. Earthq. Eng. 57, 121–132.

Rathje, E.M., Dawson, C., Padgett, J.E., Pinelli, J.P., Stanzione, D., Adair, A., Mosqueda, G., 2017. DesignSafe: New cyberinfrastructure for natural hazards engineering. Natural hazards review 18 (3), 06017001.

Roscoe, K.H., 1956. Stability of short pier foundations in sand. Br. Weld. J. 3, 343.

Taskari, O., Sextos, A.G., 2015. Probabilistic assessment of abutment-embankment stiffness and implications in the predicted performance of short bridges. J. Earthq. Eng. 150218133146008.

Waldin, J., Jennings, J., Routledge, P., 2012. Critically damaged bridges and concepts for earthquake recovery. 2012 NZSEE Conference.

Yang, Z., Elgamal, A., Parra, E., 2003. Computational model for cyclic mobility and associated shear deformation. Journal of geotechnical and geoenvironmental engineering 129 (12), 1119–1127.

Ziegler, H., 1977. An Introduction to Thermomechanics. North-Holland, Amsterdam.